Employing Imbalance Forecasts to Proactively Counteract Deterministic Frequency Deviations

Julie Rousseau*†, Johanna Vorwerk*, Iason Avramiotis‡, Christian Welti‡, Gabriela Hug*
*Power Systems Laboratory, ETH Zürich, Zürich, Switzerland
‡ Swissgrid Ltd. Aarau, Switzerland
†jrousseau@ethz.ch

***Abstract*—In power systems, discrepancies between the scheduled step-wise power production and the smooth power consumption result in volatile frequency profiles. Sudden changes at the end of each market delivery period cause Deterministic Frequency Deviations (DFDs). Literature suggests various counteracting measures, but they are insufficient to limit DFDs. We propose two methods to anticipate DFDs. Both rely on the forward activation of active power based on power imbalance forecasts. While the first method employs traditional ancillary services in a new fashion, the second one suggests a novel service to analyse the benefits of implementing regulatory changes. Both proposed solutions are compared to employing fast-frequency control services. All methods are tested on real DFDs that exhibit a considerable Swiss contribution in 2020 in Continental Europe (CE). Using a dynamic model representing Switzerland as a part of the CE grid, the presented work highlights the efficacy of the suggested forward activation of power. The results indicate a significant reduction in the DFD amplitude and costs of standard ancillary services.**

***Index Terms*—Deterministic Frequency Deviation (DFD), imbalance forecast, forward activation of power, frequency dynamics model, fast-frequency response**

I. Introduction

For many years, Transmission System Operators (TSOs) have observed repeated frequency deviations from one market interval to the next. In Synchronous Area Continental Europe (CE), producers and consumers mainly trade hourly energy blocks on the energy market [1]. However, except for large facilities, consumer profiles are relatively smooth. Consequently, power imbalances arise [2] and lead to significant frequency disruptions whenever the hour changes, as exhibited by the averaged daily frequency profile of CE for 2020 in Fig. 1.

These Deterministic Frequency Deviations (DFDs) have numerous consequences for the electric power grid. Besides the stresses they put on the physical components, DFDs repeatedly require the deployment of frequency ancillary services to counteract the imbalances [3]. Hence, the costs associated with DFDs are high. In addition, exhausting frequency reserves for DFDs could have severe consequences in case of outages [2], e.g., repeated under-frequency load sheddings [4].

Recent literature explores a variety of solutions to reduce DFDs. [5] suggests shorter market intervals. For example, $15\,\mathrm{min}$ energy markets were implemented in CE resulting in positive effects on the frequency [6]. Nevertheless, the traded volumes are insufficient to reduce DFDs [1]. Multiple authors suggest transforming the power profiles of large power plants, e.g., [2], [7]. The latter reference proposes to penalize power production steps when computing imbalances of balance groups and was implemented by the Swiss (CH) TSO in 2010. The method proved beneficial, but its implementation in CE is difficult [8]. Alternatively, [4] suggests to increase the reserved frequency control capacity as a temporary action. Despite the decrease in DFD amplitude, this method significantly increases grid operation costs. Hence, the suggested strategies either face implementation hurdles in CE or are insufficient to significantly reduce DFDs.

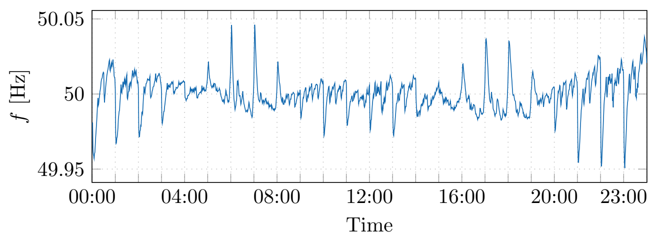

Fig. 1. Average daily frequency profile of the CE power system for 2020.

Since DFDs occur daily with recurring patterns, a proactive solution is conceivable [9]. Nevertheless, such a solution requires imbalance forecasts that are only investigated by a few studies. The authors in [10] study the variables that could affect the Czech imbalance energy over $1\,\mathrm{h}$ and successfully implement auto-regressive prediction methods, whereas [11] demonstrates the superiority of neural networks when predicting the British imbalance energy over intervals of $4\,\mathrm{h}$. Forecasting errors were also reduced by employing advanced machine learning techniques in [12], [13]. Even though some studies designed imbalance forecast methods, none provide a prediction method suitable to anticipate recurrent imbalances.

Acknowledging the aforementioned gaps and drawbacks, we suggest a forward activation of active power to reduce repeating DFDs. The proposed method relies on imbalance forecasts of a control area that are conducted before the potential imbalance occurs. We focus on the reduction of the CH contribution to DFDs in the CE power system. Hence, the contributions of this paper are three-fold:

- We provide a comprehensive analysis of the DFDs in CE in 2020, emphasising the CH contribution.
- We suggest a framework to tackle DFDs that relies on the prediction of power imbalances and employs forward activation of different standardized active power profiles. The imbalance forecast is designed using a $1\,\mathrm{s}$ resolution. Besides existing traditional services, the employment of a new ancillary service is investigated.
- We develop and employ a frequency dynamic model representing CH within the CE grid to compare the effectiveness of the proposed method against the deployment of fast-frequency reserves (FFR).

The remainder of this paper is organized as follows: *Section II* provides further insights into DFDs and the CH contribution to it. *Section III* introduces the proposed scheme for a forward activation of active power while *Section IV* briefly defines the benchmark FFR. *Section V* conducts a case study based on the CE system and displays the results for both implemented approaches. *Section VI* highlights the key outcomes and concludes the work.

II. Deterministic Frequency Deviations

DFDs are observed recurrently, endangering the stability of electric power grids. This section defines the phenomenon and evaluates the situation in CE as well as the CH contribution.

A. Definition of a DFD

A DFD is detected at hour h if there exists a set of discrete time steps $F^{\mathrm{h}} = (t_0, t_1, \ldots t_{\mathrm{N}})$ during which the frequency satisfies [14]:

$$\begin{cases} \forall t \in F^{\mathrm{h}}, \quad |f^{\mathrm{t}} - f_0| \geq 75 \text{ mHz}, \\ t_{\mathrm{N}} - t_0 \geq 15\mathrm{s}, \\ \mathrm{argmax}_{t \in F^{\mathrm{h}}} |f^{\mathrm{t}} - f_0| \in [h-1:55; h:05], \end{cases} \tag{1}$$

where f^{t} denotes the discrete frequency that is measured at time t and f_0 represents the nominal frequency.

However, this definition may count a single event multiple times when the frequency deviation oscillates around $75\,\mathrm{mHz}$. Thus, a time constraint is added: Two events are considered as a single DFD if they appear less than $5\,\mathrm{min}$ apart.

B. Contribution of a Control Zone

A power imbalance in one control area of an interconnected system results in a global frequency deviation. When power disturbances occur, the Area Control Error (ACE) of each zone y helps identifying the responsible region:

$$\mathrm{ACE}_{\mathrm{y}}^{\mathrm{t}} = \Delta P_{\mathrm{T,y}}^{\mathrm{t}} + {S_{\mathrm{y}}}^{-1} \Delta f^{\mathrm{t}}, \tag{2}$$

where S_{y} is the primary control droop coefficient of area y, $\Delta P_{\mathrm{T,y}}^{\mathrm{t}}$ denotes the difference between the planned and actual power exports of area y and Δf^{t} is the CE frequency deviation at time t. Per definition, the ACE equals an area's instantaneous power imbalance.

As the TSO is only responsible for its control area, it is crucial to assess the contribution of each control zone in a DFD. Traditionally, only one region is responsible for a large frequency deviation, e.g., after a generator blackout. However, since most of the CE energy markets mainly trade in hourly intervals, multiple control areas contribute to DFDs.

Based on the ACE, [15] defines the frequency contribution of a control zone as:

$$\mathrm{FC}_{\mathrm{y}}^{\mathrm{t}} = \frac{\mathrm{ACE}_{\mathrm{y}}^{\mathrm{t}}}{\sum_{k \in \mathcal{C}} \mathrm{ACE}_{\mathrm{k}}^{\mathrm{t}}} \Delta f^{\mathrm{t}} = \frac{\mathrm{ACE}_{\mathrm{y}}^{\mathrm{t}}}{\sum_{k \in \mathcal{C}} \frac{1}{S_{\mathrm{k}}}}, \tag{3}$$

where $\mathcal{C}$ designates the set of control zones in the CE power grid. This metric measures the share of the control area in the total power imbalance of the interconnected system. Finally, the contribution of a control zone in a DFD associated with F^{h} is defined as its maximum absolute value over F^{h}.

C. Situation in CE

DFDs cause severe and repeated frequency excursions in CE. One of the most severe incidents occurred on the 10^{th} of January 2019, when the simultaneous occurrence of a large DFD and broken measurement devices placed the CE power grid in an alert state, i.e., frequency deviations exceeded $200\,\mathrm{mHz}$, for $9\,\mathrm{s}$. Moreover, Fig. 2 illustrates the number of frequency deviations larger than $\pm 75\,\mathrm{mHz}$ for 2020. Most of these excursions, in fact $92\,\%$, qualify as DFDs. Aligned with these findings, [14] reports an increasing trend in the number and severity of DFDs in CE. As DFDs cause such a high number of incidents, it is important to further analyze them and find new solutions to tackle this issue.

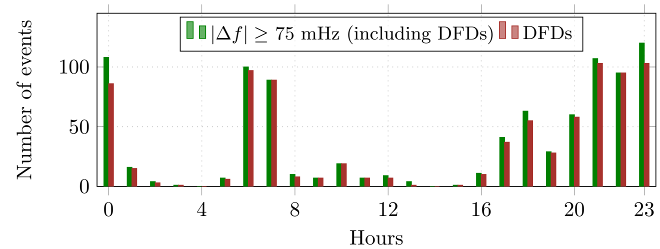

Fig. 2. Number of frequency deviations larger than $75\,\mathrm{mHz}$ and DFDs observed in 2020 in CE.

In 2020, the average CH contribution to DFDs stayed below 10%. Yet, it exceeded 20% during 26 events. Two factors may explain this. The three largest CH contributions were observed at off-peak hours or during weekends when the contributions of other countries are usually lower. Furthermore, the CH energy mix is composed of 57% of hydropower plants [16]. These generators exhibit significant ramping rates which may create large sudden imbalances at the end of trading intervals. Thus, counteracting the CH imbalances during these events with high contributions benefits the entire CE power grid. Besides, a scheme that is effective for these events, is implementable in control zones with larger average contributions.

III. Anticipating DFDs: A Forecast-Based Method

Since DFDs are caused by recurring active power mismatches around the trading interval, they may be predicted. We suggest forecasting the power imbalance to activate additional control reserves with the goal of minimizing the DFD amplitude. This section first mathematically defines active power imbalances, before suggesting two standardised profiles to proactively counteract the expected imbalance. Finally, the framework to forward activate active power is discussed.

A. Definition of a Power Imbalance

The power imbalance $P_{\mathrm{imb,y}}$ of an area is defined as the amount of reserve used to reestablish its power balance [17]:

$$P_{\mathrm{imb,y}} = P_{\mathrm{y}}^{\mathrm{mFRR}} + P_{\mathrm{y}}^{\mathrm{aFRR}} - \mathrm{ACE}_{\mathrm{y}} + P_{\mathrm{corr,y}}^{\mathrm{IGCC}}. \tag{4}$$

where $P_{\mathrm{y}}^{\mathrm{mFRR}}$ denotes the manual Frequency Restoration Reserves (mFRR) and $P_{\mathrm{y}}^{\mathrm{aFRR}}$ describes the automatic Frequency Restoration Reserve (aFRR). $P_{\mathrm{corr,y}}^{\mathrm{IGCC}}$ is the correction factor computed as part of the International Grid Control Cooperation (IGCC) and accounts for imbalances in other areas to prevent power activation in opposite directions [18]. It equals zero when the area does not participate in this collaboration.

B. Forecasts of the Imbalance

As power mismatches occur repeatedly, their daily patterns can be exploited. Averaging past data alleviates the need for extensive information from various entities. Besides, imbalances exhibit fast ramps that are only predictable with high time resolutions. Given high-resolution data, averaging past values provide a high-resolution forecast.

This section presents three different methods to forecast power imbalances. They all exploit average daily imbalance information and predict power mismatches for $40\,\mathrm{min}$ around the hour change with a $1\,\mathrm{s}$ resolution. The first method is a persistence model using the daily average and serves as a benchmark. It is further improved by a feed-forward Neural Network (fNN). The last considered algorithm employs Weighted Nearest Neighbors (WNN).

1) Persistence Model: The persistence forecast consists of an averaged superposition of N daily profiles. It smoothens time variations and only preserves dominant patterns. If the vector $\mathbf{P}_{\text{imb}}^{\mathcal{D},h}$ represents the imbalance profile around hour h of day $\mathcal{D}$, the persistence profile $\mathcal{E}_N\left(\mathbf{P}_{\text{imb}}^{\mathcal{D},h}\right)$ is:

$$\mathcal{E}_N\left(\mathbf{P}_{\text{imb}}^{\mathcal{D},h}\right) = \frac{1}{N}\sum\nolimits_{\mathcal{D}'\in\mathcal{S}_{\mathcal{D}}}\mathbf{P}_{\text{imb}}^{\mathcal{D}',h}, \tag{5}$$

where $\mathcal{S}_{\mathcal{D}}$ is the set of N past days before $\mathcal{D}$. Note that, in the rest of this paper, bold signs are used to designate vectors.

Preliminary studies showed a minimal Root-Mean Square Error (RMSE) of the persistence model on CH imbalances in 2020 when using 30 days. In addition, distinguishing weekdays and weekends proved beneficial due to substantial differences in the profiles.

2) Correction of the Persistence Model with a Feed-Forward Neural Network (fNN): A residual imbalance $\mathbf{R}_{\text{imb}}^{\mathcal{D},h}$ defined as:

$$\mathbf{R}_{\text{imb}}^{\mathcal{D},h} = \mathbf{P}_{\text{imb}}^{\mathcal{D},h} - \mathcal{E}_{30}\left(\mathbf{P}_{\text{imb}}^{\mathcal{D},h}\right), \tag{6}$$

remains when employing averaged daily profiles. Therefore, an fNN is employed to reduce the overall prediction error.

The analysis of the CH imbalance indicates that residuals are dominated by long-lasting trends rather than fast-oscillating behaviours. Thus, the residuals are forecasted with a $1\,\text{min}$ resolution instead of $1\,\text{s}$, significantly reducing the computational burden of the fNN. The reduced set of residuals $\tilde{\mathbf{R}}_{\text{imb}}^{\mathcal{D},h}$ only contains 41 instead of 2401 time steps per hour change. To match the resolution of fNN predictions and the average profiles, a smooth interpolation is employed.

Eventually, a forecast $\mathcal{F}$ for the power imbalance occurring around a specific hour and day $\mathcal{D}$ is obtained with

$$\mathcal{F}\left(\mathbf{P}_{\text{imb}}^{\mathcal{D},h}\right) = \mathcal{E}_{30}\left(\mathbf{P}_{\text{imb}}^{\mathcal{D},h}\right) + \mathcal{F}_I\left(\mathbf{R}_{\text{imb}}^{\mathcal{D},h}\right),$$

where $\mathcal{F}_I\left(\mathbf{R}_{\text{imb}}^{\mathcal{D},h}\right)$ is the smooth fNN interpolated prediction.

To select suitable features, the correlations of imbalances in CH in 2020 are studied. The following features achieved the best performance and are thus included in the method:

- the residuals of the past $15\,\text{min}$ before the event at a $1\,\text{min}$ resolution,
- the residuals around the past $3\,\text{h}$ at a $1\,\text{min}$ resolution,
- the net production step planned for the hour of interest, composed of the scheduled power production of large power plants and consumption of large pumps,
- indicators of the hour of the day, the day of the week and the month of the year.

Further analysis indicated the best performance, i.e., the lowest RMSE, for an fNN with 1 hidden layer and 20 neurons.

3) Weighted-Nearest Neighbours (WNN): The WNN technique exclusively considers days similar to the one to be predicted among potential neighbors. To define similarity between days, features that reflect the system's state before the hour of interest must be defined.

The algorithm from [19] is applied. It computes the distance $d\left(\mathbf{I}_{\mathcal{D},h}, \mathbf{I}_{\mathcal{M},h}\right)$ to $\mathcal{D}$ for every neighbour $\mathcal{M}$, where d is the Euclidean norm. Based on these distances, the algorithm determines the set of k-nearest neighbours, $\mathcal{B}_k^{\mathcal{D},h}$, as the k neighbours having the smallest distances to $\mathcal{D}$. Eventually, the WNN method forecasts the power imbalance $\mathbf{P}_{\text{imb}}^{\mathcal{D},h}$ with a weighted average of the k-nearest neighbors with:

$$\mathcal{W}_k\left(\mathbf{P}_{\text{imb}}^{\mathcal{D},h}\right) = \sum\nolimits_{\mathcal{M}\in\mathcal{B}_k^{\mathcal{D},h}} \frac{d(\mathbf{I}_{\mathcal{D},h},\mathbf{I}_{\mathcal{M},h}) - d_{min}}{d_{max}-d_{min}}\mathbf{P}_{\text{imb}}^{\mathcal{M},h}, \tag{7}$$

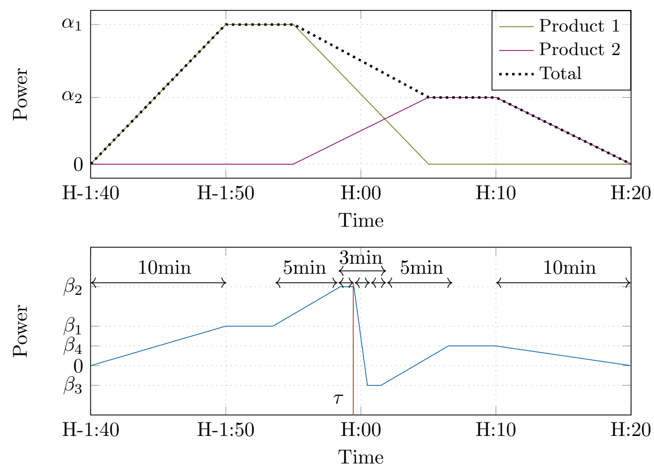

Fig. 3. Suggested standardized power profiles: Two traditional mFFR products (top) or a fast-ramping profile (bottom).

where d_{min} and d_{max} are the smallest and largest distances of the set $\mathcal{B}_{k+1}^{\mathcal{D},h}$.

Preliminary studies are performed to tune the algorithm. The same features as for the fNN are employed. All imbalance profiles of the past year around the same hour are potential neighbors. Finally, a number of 20 nearest neighbors is chosen as it minimizes the RMSE of the CH imbalance in 2020.

C. Definition of Standardized Power Profiles

One potential solution for counteracting DFDs before they occur is to activate some active power in advance based on the previously discussed imbalance forecast. To automatise this activation of active power, two standardized power profiles are suggested in this section.

1) Two manual Frequency Restoration Reserve (mFFR) Products: The mFRR profile is a good candidate for this service. It is a $15\,\text{min}$ power step. For smoothing, two ramps of $10\,\text{min}$ are included, as shown in Fig. 3. This product is characterized by the active power amplitude α.

Nevertheless, a single mFRR product is insufficient to tackle all DFDs. Indeed, DFDs appear in an interval of $10\,\text{min}$ centered around the hour change, while mFRR products occur either $15\,\text{min}$ before or after the hour change. Hence, a combination of two mFRR products is considered, where $\boldsymbol{\alpha} = (\alpha_1, \alpha_2)$ contains the two amplitudes, characterizing the overall profile.

mFRR products are convenient for several reasons. In practice, the swift change in power production at the hour generates a sudden short-lasting imbalance. But, long-lasting imbalances are observed before and after the hour change. Even if the combination of mFRR products cannot mimic abrupt imbalances at the hour, it may reduce the effect of the slow ones before and after the hour. Besides, mFFR is an existing service, thus it is easily accessible for counteracting DFDs.

2) Fast-Ramping Profile: An additional power profile is proposed to counteract both short and long-lasting imbalances. Fig. 3 displays the design of this ancillary service, characterised by four amplitudes $\boldsymbol{\beta} = (\beta_1, ..., \beta_4)$ and the starting time τ of the fast ramp. The first and last power values compensate imbalances around the hour change, while the other two capture short-lasting imbalances and adjust the amplitude of the ramp. The profile is constant for $1\,\text{min}$ before and after the fast ramp, chosen as a trade-off between a triangular shape and steady constant values around the ramp.

TABLE I
PARAMETERS FOR DROOP-BASED SERVICES.

Parameter	**Frequency-proportional**		**RoCoF-proportional**	
Time delays	T_{f}	1 s	T_{df}	1 s
Droop	$S_{\mathrm{B,f}}$	1100 MW	$S_{\mathrm{B,df}}$	1100 MW
	$S_{\mathrm{f}}^{\mathrm{pu}}$	1%	γ	1000 s
Dead Bands		±60 mHz		±2.5 mHz/s
Saturation		±150 mHz		

TSOs willing to implement such a service could decompose it into a fast-ramping product and two $15\,\mathrm{min}$ mFRR products.

D. Optimal Activation of Power Profiles

For each hour, the optimal parameters of the suggested profiles might differ. Using the imbalance forecasts, the parameters of both profiles are determined by solving an optimization problem.

Several objective functions are considered for this task. Minimising FCR and aFRR energy tends to overestimate the power compensation around the fast ramp to reduce the frequency deviation amplitude. Besides, this objective requires computing the expected aFRR and FCR energy, which is computationally intensive. Furthermore, a minimisation of the aFRR energy over-corrects the imbalance of small zones. Thus, for both profiles the parameters are optimised to minimise the expected imbalance energy of the entire system.

1) Two mFFR Products: The optimal parameters $\boldsymbol{\alpha}^{*}$ are selected such that the imbalance energy over the $40\,\mathrm{min}$ interval around the hour of interest $\mathcal{T}_{\mathcal{D},h} = [h\text{-}1{:}40{:}00;\ h{:}20{:}00]$ is minimised, i.e.,

$$\begin{aligned} \min_{\boldsymbol{\alpha}\in\mathbb{R}^2} \int_{t\in\mathcal{T}_{\mathcal{D},h}} \left| \mathcal{X}\left(\mathbf{P}_{\mathrm{imb}}^{\mathcal{D},h}\right)(t) - \mathbb{T}(t;\boldsymbol{\alpha}) \right| \mathrm{d}t, \\ \text{subject to} \quad \alpha_{\min} \leq \boldsymbol{\alpha} \leq \alpha_{\max}, \end{aligned} \tag{8}$$

where $\mathcal{X}\left(\mathbf{P}_{\mathrm{imb}}^{\mathcal{D},h}\right)(t)$ denotes the predicted power imbalance and $\mathbb{T}(t;\boldsymbol{\alpha})$ the power of the selected profile.

2) Fast-Ramping Profile: Before optimizing the fast-ramping profile's amplitudes, the time τ^{*} is selected as the beginning of the $1\,\mathrm{min}$ interval in which the absolute power gradient of the imbalance forecast is the largest, i.e.,

$$\tau^{*} = \mathrm{argmax}_{k\in\Omega} \left| \sum_{i=1}^{60} \left(\Delta\mathcal{X}\left(\mathbf{P}_{\mathrm{imb}}^{\mathcal{D},h}\right)/\Delta\mathrm{t} \right)(k+i) \right|, \tag{9}$$

with $\Omega = [h\text{-}1{:}56{:}00;\ h{:}03{:}00]$. Then, the four optimal power amplitudes are selected as follows:

$$\begin{aligned} \min_{\boldsymbol{\beta}\in\mathbb{R}^4} \int_{t\in\mathcal{T}_{\mathcal{D},h}} \left| \mathcal{X}\left(\mathbf{P}_{\mathrm{imb}}^{\mathcal{D},h}\right)(t) - \mathbb{T}(t;\boldsymbol{\beta},\tau^{*}) \right| \mathrm{d}t, \\ \text{subject to} \quad \beta_{\min} \leq \boldsymbol{\beta} \leq \beta_{\max}. \end{aligned} \tag{10}$$

IV. BENCHMARK: FAST FREQUENCY RESPONSE (FFR)

In low inertia systems, FFR services are capable of reacting to sudden imbalances within seconds. As such, FFR services are increasingly incorporated in reduced inertia and small power systems. Similar to primary control, these services typically provide a response proportional to the frequency deviation or the Rate of Change of Frequency (RoCoF). In modern systems, they might be an alternative solution to tackle DFDs without the need for additional services. Thus, frequency- and RoCoF-proportional services provide a benchmark for the case studies.

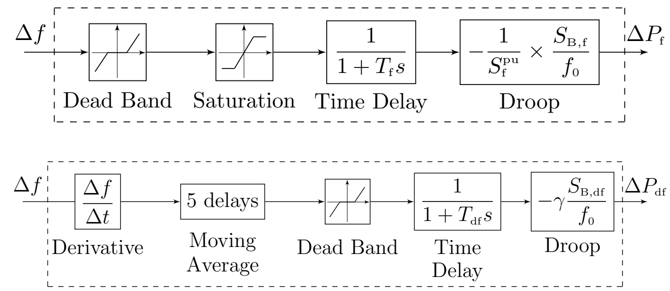

Fig. 4. Block-diagrams of the FFR: Frequency-proportional response (top) and RoCoF-proportional response (bottom).

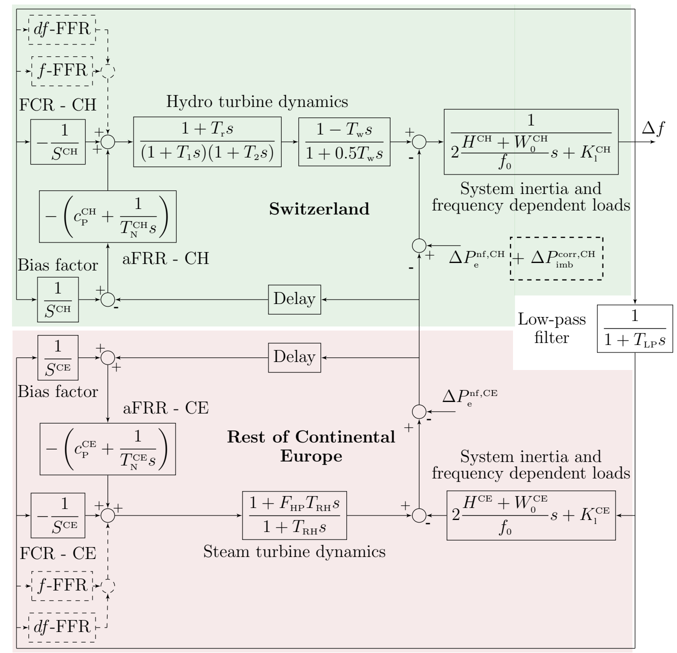

Fig. 5. Block diagram for studying frequency dynamics composed of CH (green) and the rest of CE (red). The dashed blocks represent the different methods implemented in this paper.

Both services are implemented as detailed in Fig. 4. While both are based on proportional control, usually referred to as droop control, the RoCoF-based service first measures the RoCoF with a derivative block and a moving average. Table I provides the parameters that are adapted from [20].

V. CASE STUDIES

Case studies are performed to assess the effectiveness of the proposed forward-activation of power against the benchmark FFR services. First, a frequency dynamic model that assesses the impact of both methods on the amplitude of DFDs and the CH contribution is presented. This section then introduces the test setup, before displaying and discussing the results.

A. Frequency Dynamics Model

The frequency dynamics model displayed in Fig. 5 is employed for the case studies. It contains two areas: CH and the rest of the CE grid.

The swing equation governs each area of the system. Considering their energy mix, CH is represented by a hydro turbine and the rest of CE by a steam turbine. Details on the turbine dynamics can be found in [21]. Both areas provide standard primary and secondary frequency control.

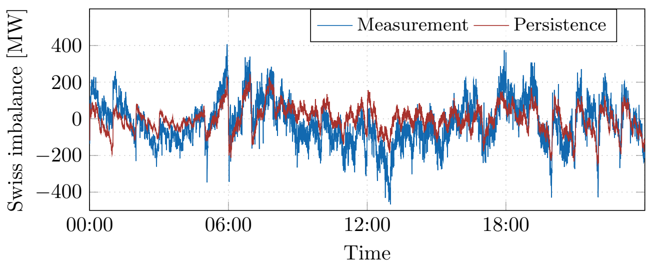

Fig. 6. Approximation of the CH power imbalance by the average daily profile of the thirty past weekdays.

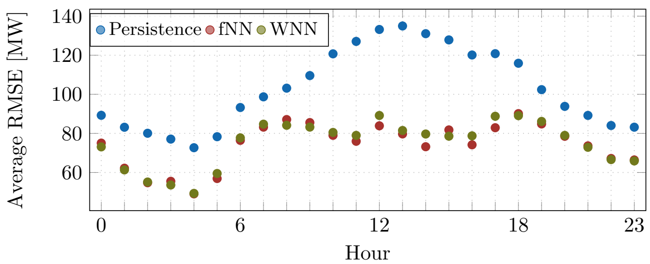

Fig. 7. Evolution of the average RMSE of the different models throughout the hours of the day.

TABLE II
AVERAGE RMSE OF THE IMBALANCE FORECASTING METHODS.

Technique	Persistence	fNN	WNN
Average RMSE	102.89 MW	74.87 MW	74.88 MW

The reduction method proposed in [22] is applied to omit inter-area oscillations and a unique frequency for the entire system is assumed: $f_{\text{CE}} \approx f_{\text{CH}} \approx f$.

As such, the simulated grid frequency emulates the inertial, FCR, and aFRR responses in the rest of CE. These power adjustments are transmitted to CH through cross-border lines. As the ACE accounts for cross-border exchanges, the model includes an algebraic loop, which may not converge. Thus, a unit delay is added to the cross-border flows to enhance numerical stability.

The model parameters are determined based on previous studies and internal information provided by the Swiss TSO. They are further adjusted to fit the frequency measurements during three significant power plant outages in CH.

B. Forecast of the CH Power Imbalance

Before assessing the performance of the DFD prevention tools, the accuracy of the imbalance forecast is demonstrated.

Fig. 6 displays the time-domain performance of the persistence method for an exemplary day. The daily average captures the sudden hourly power changes causing DFDs. Consequently, the residual imbalance, that is the difference between both provided curves, oscillates around zero and barely exhibits hourly patterns.

Table II compares the algorithm performances in terms of RMSE. Each algorithm is trained on CH power imbalances from 2019 and then evaluated on 2020 data. The persistence profile exhibits the highest forecasting error. It only accounts for imbalances that follow daily patterns. The correction of the persistence by an fNN outperforms the benchmark by about 30 MW. The WNN performance is similar.

Fig. 7 displays the hourly RMSE of each algorithm. While the persistence forecast is competitive at hours dominated by deterministic patterns, such as the night, its RMSE during

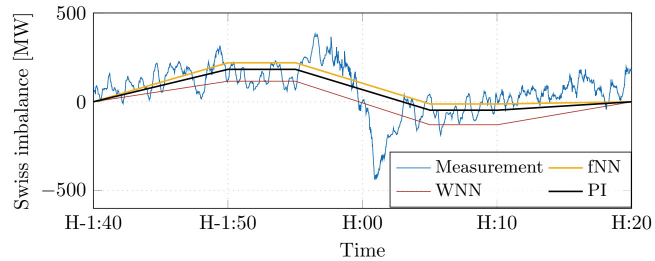

Fig. 8. Optimal power activation of two mFRR products during a DFD event. The activation of power relies on the fNN and WNN forecasts, and on PI.

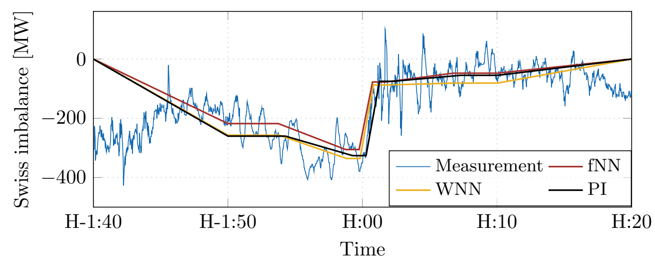

Fig. 9. Optimal power activation of the fast ramping product during a DFD event. The activation of power relies on the fNN and WNN forecasts, and on PI.

the day dramatically increases. The persistence model cannot capture the external factors that influence the imbalances during the day. The fNN and WNN show better performances and similar to each other. Since both account for externalities, they perform particularly well when the daily average fails.

As the fNN and WNN forecasts yield similar results, the non-linearity added by the fNN may not be required to predict imbalance at the end of hourly trading intervals.

C. Comparison of the DFD prevention schemes

To assess and compare the DFD prevention schemes presented in this paper, a set of 26 DFDs in CE is selected. Each event contains $40\,\text{min}$ around an hour in 2020, and exhibits a relative CH contribution larger than 20%.

1) Metrics: A few additional metrics are defined to evaluate the different prevention mechanisms. The goal is to reduce the amplitude of the frequency deviation at the end of each market interval. However, the RoCoF is also an important metric as it indicates how fast power generators ramp up at the hour change. Therefore, both indicators are considered. Moreover, counteracting DFDs should also reduce the usage of traditional ancillary services. Since TSOs reward power producers for the aFRR energy produced, the reductions of aFRR energy and cost are investigated. Finally, the power profiles are optimised based on forecasts and may be sub-optimal due to imperfect information. Hence, the actual optimal profile is computed a posteriori with perfect information (PI), i.e., based on measurements of the CH imbalance.

2) Benchmark - Droop-Based Services: FFR reacts faster than a standard primary droop control to a power imbalance and thereby limits the frequency deviation. As such, this benchmark solution reduces the amplitude of the frequency deviation by 2.7% on average. Limited benefits are observed for the RoCoF, i.e., 1.1%. Additionally, FFR reduces the CH contribution by only 0.37% on average.

Implementing an additional RoCoF-proportional service produces synthetic inertia that retards the dynamics. Out of the 26 cases, combining both services reduces the frequency deviation by 2.7% and the RoCoF by 6.9% on average. In

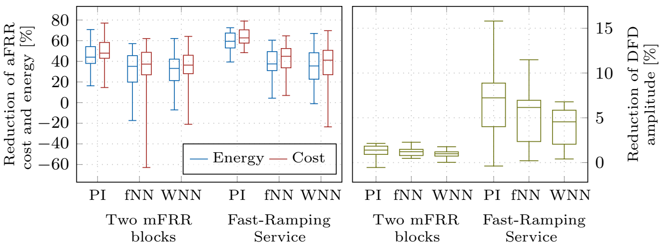

Fig. 10. Reduction of the DFD amplitude and the aFFR cost and energy over the set of 26 cases. A negative reduction signifies an increase.

short, adding a RoCoF proportional service significantly reduces the RoCoF, but only slightly lowers the DFD amplitude.

3) Forward Activation of Active Power with PI: Fig. 8 and 9 illustrate examples for the compensation of imbalances by mFRR products and fast-ramping profiles for different imbalance forecasts and the assumption of PI. Using mFFR reduces the imbalance around the swift ramp, but cannot counteract the swift power drop at the hour change, as suggested by Fig. 8. However, in Fig. 9, the fast-ramping power profile additionally counteracts sudden imbalances when the hour changes.

Fig 10 provides a boxplot of the metrics for all 26 DFD incidents contained in the test set. The CH contribution is omitted to enhance readability. Using mFRR products yields significant benefits. With PI, it reduces the aFRR energy used by 43.96% and the DFD amplitude by 1.28% on average. Nevertheless, a fast-ramping profile leads to better results for all metrics. It especially helps reducing DFD amplitudes: on average by 6.79%. Consequently, the suggested fast-ramping profile clearly outperforms all other solutions, with PI.

4) Impact of Forecasts: Since the real-time forward activation of power relies on forecasts, evaluating the metrics in this set-up is necessary and additionally provides a comparison of the predictions. With mFRR products, the WNN and fNN forecasts reduce the amount of aFRR energy used by 31.26% and 31.44%, and the DFD amplitudes by 0.99% and 1.24%, on average. Reductions of a similar order of magnitude are observed for the CH aFRR energy costs. With a fast ramping profile, the fNN and WNN reduce the amount of aFRR energy used by 38.90% and 34.97%, and the DFD amplitudes by 5.14% and 4.06%, on average. Therefore, both forecast methods seem to yield similar results, on average.

Fig 10 also presents the spread of the metrics for each case. It indicates that a forward activation of mFFR products, based on forecasts, would increase the used aFRR energy, compared to the actual one, in a few cases. Nevertheless, this risk seems to diminish when activating a fast-ramping power profile. Indeed, the activation of this profile based on the fNN forecast yields performance benefits in all 26 cases, while 2 cases yield worst performances with WNN. Hence, it indicates the superiority of fNN on the presented test set.

VI. Conclusion

This work demonstrates the efficacy of a forward activation of power to reduce DFDs. Contrary to employing FFR, activating power in advance not only reduces the DFD amplitude, but also reduces the amount of aFRR energy used. The observed frequency improvements are of the same order or higher than those obtained with FFR. Indeed, FFR does not capture the deterministic aspect of DFDs and aims at increasing the flexibility of TSOs to withstand imbalances. By anticipating imbalances, a forward activation of power is favorable.

Even though the presented work clearly demonstrates the superiority of a fast-ramping power profile, it also illustrates the significant benefits of activating $15\,\mathrm{min}$ mFRR products, mainly in reducing the aFRR energy to be used. Since such a power profile already exists in CE ancillary services markets, it is an easily accessible solution for grid operators to increase the grid's reliability and reduce costs.

The two advanced forecasting methods exhibit similar outcomes. The slight differences observed on individual cases are insufficient to declare one of them as superior. As such, the non-linearity of the fNN does not bring significant improvements. Besides, the WNN only requires tuning the number of nearest neighbours and seems, therefore, most appropriate to forecast imbalances at the end of hourly market intervals.

Although this paper provides encouraging results on the reduction of DFDs, further studies are required to assess the performances on a broader set of events, particularly, cases where the CH contribution is low. Besides, the implementation of the proposed method in other control areas, with higher contribution to DFDs, is of interest. Eventually, the implementation of such methods from TSOs requires further investigation of the market design. TSOs should ensure the willingness of producers to repeatedly deliver $15\,\mathrm{min}$ mFRR products. On the other hand, a novel market setup should be researched before implementing a fast-ramping power profile.

References

[1] EpexSpot, "New record volume traded on EPEX SPOT in 2020," 2020.

[2] T. Weißbach and E. Welfonder, "High Frequency Deviations within the European Power system - Origins and Proposals for Improvement," *VGB PowerTech*, vol. 89, no. 6, 2009.

[3] ENTSO-E, "Deterministic Frequency Deviations - Root Causes and Proposals for Potential Solutions," 2011.

[4] Elia, "Report on Deterministic Frequency Deviations: Lowering the contribution of the Belgian Control Block," 2020.

[5] S. Remppis, F. Gutekunst, T. Weißbach, and M. Maurer, "Influence of 15-minute contracts on frequency deviations and on the demand for balancing energy," *International ETG Congress*, 2015.

[6] T. Weißbach, S. Remppis, and H. Lens, "Impact of Current Market Developments in Europe on Deterministic Grid Frequency Deviations and Frequency Restoration Reserve Demand," *International Conference on the European Energy Market*, 2018.

[7] Nordic Operations Development Group (NOD), "Evaluation of the Ramping Restriction in the Energy Market," 2010.

[8] ENTSO-E, "Report on Deterministic Frequency Deviations," 2019.

[9] I. Avramiotis-Falireas, A. Troupakis, F. Abbaspourtorbati, and M. Zima, "An MPC strategy for automatic generation control with consideration of deterministic power imbalances," *Proceedings of IREP Symposium: Bulk Power System Dynamics and Control*, 2013.

[10] S. Kratochvíl, *System Imbalance Forecast*. PhD thesis, Czech Technical University in Prague, Department of Economics, Management and Humanities, 2016.

[11] M. Garcia and D. Kirschen, "Forecasting system imbalance volumes in competitive electricity markets," *IEEE Trans. Power Syst.*, vol. 21, no. 1, 2006.

[12] T. S. Salem, K. Kathuria, H. Ramampiaro, and H. Langseth, "Forecasting intra-hour imbalances in electric power systems," *AAAI Conference on Artificial Intelligence*, 2019.

[13] J.-F. Toubeau, J. Bottieau, Y. Wang, and F. Vallee, "Interpretable Probabilistic Forecasting of Imbalances in Renewable-Dominated Electricity Systems," *IEEE Trans. Sustain. Energy*, 2021.

[14] ENTSO-E, "Continental Europe Significant Frequency Deviations," 2019.

[15] ENTSO-E, "LFC Report 2019: Regular Report of the Performance of the Primary and Secondary Load-Frequency control." Restricted access.

[16] Swiss Federal Office of Energy, "Hydropower," 2021.

[17] ENTSO-E and Business & Decision, "ACE prediction project - Exploratory Data Analysis." Restricted access, 2018.

[18] Swissgrid, "Factsheet: International Grid Control Cooperation," 2021.

[19] J. Kruse, B. Schäfer, and D. Witthaut, "Predictability of Power Grid Frequency," *IEEE Access*, vol. 8, 2020.

[20] L. Toma *et al.*, "On the virtual inertia provision by BESS in low inertia power systems," in *IEEE International Energy Conference*, 2018.

[21] P. Kundur, *Power system stability and control*. EPRI power system engineering series, New York: McGraw-Hill, 1994.

[22] T. Weckesser and T. Van Cutsem, "Equivalent to represent inertial and primary frequency control effects of an external system," *IET Generation, Transmission and Distribution*, vol. 11, no. 14, 2017.